NEOPLASIA
www.neoplasia.com

Volume 14 Number 11 November 2012 pp. 994–1004 994

Genetic and Pharmacologic Inhibition of Complement Impairs Endothelial Cell Function and Ablates Ovarian Cancer Neovascularization[1]

Selene Nunez-Cruz*, Phyllis A. Gimotty†, Matthew W. Guerra†, Denise C. Connolly‡, You-Qiang Wu§, Robert A. DeAngelis§, John D. Lambris§,2, George Coukos*,2 and Nathalie Scholler*,2

*Penn Ovarian Cancer Research Center, Department of Obstetrics and Gynecology, University of Pennsylvania, Philadelphia, PA; †Center for Clinical Epidemiology and Biostatistics, Department of Biostatistics and Epidemiology, University of Pennsylvania, Philadelphia, PA; ‡Developmental Therapeutics Program, Fox Chase Cancer Center, Philadelphia, PA; §Department of Pathology and Laboratory Medicine, University of Pennsylvania, Philadelphia, PA

Abstract

Complement activation plays a critical role in controlling inflammatory responses. To assess the role of complement during ovarian cancer progression, we crossed two strains of mice with genetic complement deficiencies with transgenic mice that develop epithelial ovarian cancer (Tg*MISIIR-TAg*). Tg*MISIIR-TAg* mice fully or partially deficient for complement factor 3 (C3) (Tg^+C3^{KO} and Tg^+C3^{HET}, respectively) or fully deficient for complement factor C5a receptor (C5aR) (Tg^+C5aR^{KO}) develop either no ovarian tumors or tumors that were small and poorly vascularized compared to wild-type littermates (Tg^+C3^{WT}, Tg^+C5aR^{WT}). The percentage of tumor infiltrating immune cells in Tg^+C3^{HET} tumors compared to Tg^+C3^{WT} controls was either similar (macrophages, B cells, myeloid-derived suppressor cells), elevated (effector T cells), or decreased (regulatory T cells). Regardless of these ratios, cytokine production by immune cells taken from Tg^+C3^{HET} tumors was reduced on stimulation compared to Tg^+C3^{WT} controls. Interestingly, $CD31^+$ endothelial cell (EC) function in angiogenesis was significantly impaired in both $C3^{KO}$ and $C5aR^{KO}$ mice. Further, using the C5aR antagonist PMX53, tube formation of ECs was shown to be C5a-dependent, possibly through interactions with the $VEGF_{165}$ but not $VEGF_{121}$ isoform. Finally, the mouse $VEGF_{164}$ transcript was underexpressed in $C3^{KO}$ livers compare to $C3^{WT}$ livers. Thus, we conclude that complement inhibition blocks tumor outgrowth by altering EC function and $VEGF_{165}$ expression.

Neoplasia (2012) 14, 994–1004

Abbreviations: EOC, epithelial ovarian cancer; C3, complement factor 3; MDSC, myeloid-derived suppressor cell; AMD, age-related macular degeneration; ROP, retinopathy of prematurity; VEGF, vascular endothelial growth factor; ECs, endothelial cells; MISIIR, Müllerian inhibiting substance type II receptor; C5aR, complement factor 5a receptor; WT, wild type; $C3^{KO}$, C3 deficient; $C5aR^{KO}$, C5aR deficient; Tg^+, Tg*MISIIR-Tag* transgenic mice; Tg^+C3^{WT}, Tg*MISIIR-Tag* mice wild-type for C3; Tg^+C5aR^{WT}, Tg*MISIIR-Tag* mice wild-type for C5aR; Tg^+C3^{KO}, Tg*MISIIR-Tag* mice deficient for C3; Tg^+C5aR^{KO}, Tg*MISIIR-Tag* mice deficient for C5aR; Tg^+C3^{HET}, Tg*MISIIR-Tag* mice heterozygote for C3; Tg^+C5aR^{HET}, Tg*MISIIR-Tag* mice heterozygote for C5aR; mAb, monoclonal antibody; FOV, field of view; HMECs, human mammary epithelial cells; ECGS, endothelial cell growth supplement; GAPDH, glyceraldehyde-3-phosphate dehydrogenase

Address all correspondence to: Dr Nathalie Scholler, 3400 Civic Center Blvd, TRC 08-102 Penn Ovarian Cancer Research Center, Department of Obstetrics and Gynecology, University of Pennsylvania, Philadelphia, PA 19104. E-mail: naths@mail.med.upenn.edu

[1]This article refers to supplementary material, which is designated by Figure W1 and is available online at www.neoplasia.com.

[2]Co-supervised this work.

Received 2 August 2012; Revised 21 September 2012; Accepted 27 September 2012

DOI 10.1593/neo.121262

Introduction

Tumor development is a multistep process of cumulative genetic alterations that lead to cell autonomy. Inflammatory mechanisms are thought to play a critical role in this process [1,2]. Lung, skin, gastrointestinal, liver, urinary, cervical, and ovarian cancers are all associated with chronic inflammation, and attenuating such inflammation has proved beneficial in the clinical setting [3–5]. Epithelial ovarian cancer (EOC), the fifth leading cause of cancer death among women in the United States, is also intimately related to inflammation. Incessant ovulation, a purported cause of malignant transformation in the ovarian surface epithelium, is associated with the activation of cytokine networks and repair mechanisms in ovarian stroma, whereas pelvic inflammatory conditions, including endometriosis, predict an increased risk of ovarian cancer [6,7]. An early increase in serum inflammatory cytokines is detected in ovarian cancer patients [8], and ovarian tumors and ascites are characterized by a brisk inflammatory milieu [9–11]. Finally, elevated levels of complement anaphylatoxins suggestive of local complement activation have been observed in ovarian cancer patients' ascites [12]. The complement system is comprised of serum proteins, membrane-bound receptors, and regulatory proteins [13,14]. Its effector functions in host defense and inflammation are mediated mainly through the sequential activation and proteolytic cleavage of a series of serum proteins. Complement activation occurs through three distinct activation routes, the alternative, classic, and lectin pathways, all of which converge at a critical step: the activation of complement factor 3 (C3) by C3 convertase-mediated cleavage [14]. Complement functions include pathogen opsonization, inflammation mediated by C3a and C5a complement anaphylatoxins, and cytolysis resulting from the assembly of the membrane attack complex on targeted cells. Eliminating C3 prevents complement cascade activation and the generation of complement effectors that mediate a wide array of functions [13–15]. We demonstrated a role for complement activation in promoting the growth of transplanted tumors through myeloid-derived suppressor cell (MDSC) recruitment and activation in mice [16], but the role of complement in early oncogenic events remains unknown.

Complement proteins are well established as important effectors in pathologic neovascularization in age-related macular degeneration (AMD [17]), diabetic retinopathy, and retinopathy of prematurity [18], as well as in the regulation of the angiogenic factors required for normal placental development [19,20]. AMD involves a process whereby inappropriate angiogenesis in the choroid causes vascular invasion into the adjacent retina (choroidal neovascularization); preclinical models of AMD directly link complement to this process as complement components C3a and C5a promote choroidal neovascularization [21] and C5a increases vascular endothelial growth factor (VEGF) secretion of human retinal pigment epithelial cells [17]. Neovascularization is also a critical contributor to solid tumor progression, including cases of ovarian cancer [22]. VEGF, first identified as a vascular permeability factor secreted by tumor cells [23], plays a principal role in angiogenesis by stimulating migration and proliferation of endothelial cells (ECs) and the expression of angiogenesis-related genes in ECs. Alternative splicing of the *VEGF* gene gives rise to multiple isoforms, including 121, 165, 189, and 206 amino acid long products that are differentially expressed in a variety of human tissues and tumors [24,25]. Individual VEGF isoforms may differentially contribute to tumor vascularization according to the gradient model of Grunstein et al. [26] with $VEGF_{120}$ ($VEGF_{121}$ mouse homologue) recruiting peripheral vessels, $VEGF_{188}$ ($VEGF_{189}$ mouse homologue) promoting tumor neo-angiogenesis, and $VEGF_{164}$ ($VEGF_{165}$ mouse homologue) affecting intermediate structures. The importance of VEGF in tumor-associated angiogenesis is well established: overexpression of membrane-bound $VEGF_{121}$ and $VEGF_{165}$ was linked to tumor-associated intracerebral hemorrhage [27–29]; in a breast cancer xenograft model, $VEGF_{121}$ was described as the most potent tumor angiogenic factor; and soluble $VEGF_{189}$ expression in human colon, renal, and lung cancers was strongly associated with increased microvessels, cancer metastasis, and poor prognosis [30,31]. Notably, high levels of $VEGF_{165}$ have been associated with reduced survival in ovarian cancer [32], and a phase 3 clinical trial showed that Bevacizumab, a humanized monoclonal antibody (mAb) that inhibits VEGF-A, improves progression-free survival in women with ovarian cancer [33]. Although both complement activation and neo-angiogenesis play critical roles for ovarian cancer development, direct effects of complement activation on tumor neo-angiogenesis remain poorly understood.

To address this gap in knowledge, we crossed C3-deficient ($C3^{KO}$) mice [34] or complement factor 5a receptor–deficient ($C5aR^{KO}$) mice [35] with C57BL/6 Tg*MISIIR-TAg* transgenic mice that spontaneously develop EOC [36–38]. The immediate-early region of the SV40 virus that contains the oncogenic large and small T-antigen genes (*TAg* and *tag*, respectively) has been extensively used in the development of transgenic mouse models of cancer [39–42]. SV40-TAg models have revealed much about tumor biology, permitting significant advancements in the understanding of the "angiogenic switch" [43–45] and tumor progression and invasion [46]. Expression of TAg results in the functional inactivation of the critical tumor suppressor proteins p53 and Rb. In fact, mutation and/or loss of *TP53* is the most frequent genetic alteration identified in EOC, particularly the serous subtype [47,48], and mutation and/or loss of *Rb* and its downstream signaling mediators is also common [36,37,49,50]. Consistent with this fact, the expression of SV40 under the transcriptional control of the Müllerian inhibiting substance type II receptor (MISIIR) gene promoter triggers spontaneous ovarian cancer development in transgenic mice. SV40 TAg–induced ovarian cancer closely resembles the histotype of serous EOC, the most common EOC histotype in humans [36]. We report that C3 and C5aR deficiencies resulted in profoundly impaired EOC growth, reduced tumor vascularization, and inhibition of specific VEGF isoforms, revealing a novel mechanism of VEGF regulation by complement anaphylatoxin C5a.

Materials and Methods

Mice

All mouse experiments were approved by the Institutional Animal Care and Use Committee of the University of Pennsylvania and conducted according to guidelines of the National Institutes of Health. C57BL/6 Tg*MISIIR-TAg* transgenic mice [36], $C3^{KO}$ (B6.129S4-*C3*^{tm1Crr}/J) mice [34], and $C5aR^{KO}$ (*C5ar1*^{tm1Cge}/J) mice [35] have been described. Mice were housed in a barrier animal facility of the University of Pennsylvania on a 12-hour light/dark cycle. Water and standard rodent diet were provided *ad libitum*.

C57BL/6 Tg*MISIIR-TAg* mice develop spontaneous bilateral serous ovarian tumors and have a mean life expectancy of 151.6 days (~22 weeks) [36]. The ovarian cancer phenotype is transmitted as a dominant trait with 100% penetrance. Tg*MISIIR-TAg* females are infertile; therefore, mice are propagated by crossing Tg*MISIIR-TAg* males with wild-type (WT) littermate females.

Both C57BL/6 $C3^{KO}$ (B6.129S4-*C3*^{tm1Crr}/J) and $C5aR^{KO}$ (*C5ar1*^{tm1Cge}/J) mice are viable and fertile but have impaired immune responses.

To obtain Tg*MISIIR-TAg* transgenic female mice deficient for C3 (Tg^+C3^{KO}) or C5aR (Tg^+C5aR^{KO}), we crossed Tg*MISIIR-TAg* males with $C3^{KO}$ or $C5aR^{KO}$ females. Tg*MISIIR-TAg* males heterozygous for C3 (Tg^+C3^{HET}) or C5aR (Tg^+C5aR^{HET}) were then crossed with females homozygous for C3 or C5aR. The litters were sparse and small (less than or equal to five pups), consistent with an earlier report describing early pregnancy impairment in $C3^{KO}$ mice [51]. Genotyping was performed by polymerase chain reaction (PCR) using previously described primers [35,36] (Figure W1, *E* and *F*).

Immunohistochemistry and Immunofluorescence

Ovaries and ovarian tumors were collected from 16-week-old mice and preserved in optimal cutting temperature (OCT) media embedding (Tissue-Tek; Sakura Finetek USA, Torrance, CA). Sections (8 μm) were cut, air-dried for 1 hour at room temperature, and fixed by immersion in cold 100% acetone for 5 minutes. After two washes in phosphate-buffered saline (PBS), slides were blocked with goat serum (Vector Labs, Burlingame, CA). ECs were stained with a rat anti-mouse CD31 mAb (BD Pharmingen, San Jose, CA) followed by biotinylated polyclonal goat anti-rat IgG (BD Pharmingen) and detected with the VectaStain ABC reagent and DAB (Vector Labs). Microvessels were defined as any dark-stained ECs or cell clusters clearly separated from adjacent structures, tumor cells, and other connective tissue elements. Microvascular density was expressed as the number of vessels per field of view. C3 deposition was detected with a rat anti-mouse C3b/iC3b/C3c mAb (2/11; HyCult) followed by Alexa 488–labeled goat anti-rat anti-IgG1 mAb (Invitrogen). The values reported reflect C3b/iC3b deposition per cell, averaged from five field-of-view tumors. Adjacent sections were stained with hematoxylin and eosin for histopathologic evaluation.

Cell Preparation and Antibodies

Ovaries and ovarian tumors from WT, Tg*MISIIR-TAg*, Tg^+C3^{WT}, Tg^+C3^{HET}, Tg^+C3^{KO}, Tg^+C5aR^{WT}, Tg^+C5aR^{HET}, and Tg^+C5aR^{KO} mice were collected in ice-cold Dulbecco's modified Eagle's medium supplemented with 10% (vol/vol) FBS and 1% penicillin/streptomycin and mechanically dissociated using a cell strainer (BD Biosciences, San Jose, CA). Red blood cells were eliminated with ammonium-chloride-potassium (ACK) lysing buffer (Gibco, Grand Island, NY). Freshly isolated single-cell (WT, Tg^+C3^{WT}, Tg^+C3^{HET}, and Tg^+C3^{KO}) or frozen suspensions (95% FBS and 5% DMSO, stored at −80°C for up to 4 months; Tg^+C5aR^{WT}, Tg^+C5aR^{HET}, and Tg^+C5aR^{KO}) were first incubated with rat anti-mouse CD16-CD32 (2.4G2) mAb to block Fc receptors, and mouse leukocyte labeling was performed by incubation with fluorochrome-conjugated rat anti-mouse CD3 (17A2), CD4 (L3T4), CD8 (53-6.7), CD11b (M1/70), CD45 (30-F11), CD45R (B220), CD19 (ID3), F480 (BM8), or Gr-1 (RB6-8C5) Abs, at 4°C for 30 minutes. Isotype-matched antibodies were used as negative controls. For intracellular analysis of cytokines, cells were permeabilized with Cytofix/Cytoperm and Perm/Wash buffers (BD Biosciences) and stained with fluorochrome-conjugated rat anti-mouse interleukin-10 (IL-10), IL-12 (p40/p70), interferon-gamma (IFN-γ), or FoxP3 (FJK-16a) Abs. All Abs were purchased from BD Biosciences.

For intracellular analysis of cytokines, single-cell suspensions of whole mouse tumor (5×10^6) were first cultured for 24 hours at 37°C in 5% CO_2. Cells were then resuspended in fresh medium with 0.002% 2-β-mercaptoethanol (Sigma, St Louis, MO) for 4 hours in 5% CO_2. In some cases, cells were stimulated with lipopolysaccharide (LPS; 1 μg/ml) and IFN-γ (10 ng/ml) plus monensin (4 μl/6 ml of cell culture). For T-cell activation, 20 μl of anti-CD3/anti-CD28 activation beads were added per milliliter of culture as recommended by the manufacturer (Miltenyi, Auburn, CA).

In Vivo *Angiogenic Assays*

Growth factor–reduced Matrigel was mixed at 4°C (liquid state) at a 1:1 ratio with 10 ng/ml VEGF-A human recombinant homodimer protein (Millipore, Billerica, MA) or PBS as negative control. C57BL/6 WT mice were injected with 100 μl of each mixture in the right and left flanks. Animals were sacrificed 2 weeks after injection. Matrigel plugs were excised and digested with 1 mg/ml collagenase II and 10,000 U/ml DNAse I (Sigma) for 30 minutes at room temperature, as described [52], then resuspended in PBS and analyzed by flow cytometry for the expression of CD31 and CD144.

Tube Formation

Tube formation assays measure the ability of ECs to form capillary-like tubes. Human mammary epithelial cells (HMECs; 2×10^6) at passages 2 to 6 were cultured in a T75 cm^2 flask in HMEC medium [MDCB131 medium (Gibco) supplemented with 10% (vol/vol) FBS, 1% penicillin/streptomycin, 100 μg/ml endothelial cell growth supplement (ECGS), and heparin (Sigma)]. The following day, cells were starved for 1 hour in MDCB131 medium and then harvested, and 2×10^5 cells/well were incubated in Matrigel 24-well plates (BD) with 2 nM C5a native protein or human recombinant proteins VEGF-A ($VEGF_{165}$ homodimer) at 2 ng/ml, $VEGF_{165}$ single domain (35.0 MWt, Peprotech, Rocky Hill, NJ) at 2 ng/ml (57 nM) or 2.7 ng/ml (77 nM), or $VEGF_{121}$ single domain (25.4 MWt, Peprotech) at 2 ng/ml (78 nM), in the presence or absence of 100 × PMX53 (AcF[OPdChaWR]) or of a chemically similar control peptide (AcF[OPdChaA(d)R]) that lacks functional properties. Plates were incubated at 37°C for 4 hours and endothelial tube formation was examined using a light microscope (Nikon, Melville, NY) at ×10 magnification. Tube formation per area was analyzed using ImagePro software (Media Cybernetics, Rockville, MD). Experiments were repeated three times.

VEGF Isoform-specific Reverse Transcription–PCR

RNAs were extracted using Trizol reagent from 2×10^5 HMECs or from single-cell suspension of mouse organs. HMECs were cultured at 2×10^5 cells/well in HMEC medium alone or supplemented with C5a native protein (10,400 MWt, CompTech, Tyler, TX) at 2 nM (20.8 ng/ml), and/or VEGF-A (1 ng/ml), with or without PMX53 C5a inhibitor or PMX53 control peptide in 12-well plates for 24 hours. Mouse spleen, liver, and bone marrow tissues were collected from C57BL/6, $C3^{KO}$, or $C5aR^{KO}$ mice. mRNAs were reverse transcribed using M-MLV Reverse Transcriptase (Promega, Madison, WI). Human and mouse VEGFs, human β_2-microglobulin, and mouse glyceraldehyde-3-phosphate dehydrogenase (GAPDH) primers and PCR conditions were used as described [53]. Densitometry analysis was performed using ImageJ software (Image processing and analysis in Java) freely available from the National Institutes of Health at http://rsb.info.nih.gov/ij. Experiments were repeated three times.

Statistical Analyses

The data from experiments with two groups were analyzed using Student's *t* test and data from experiments with more than two groups were analyzed using one-way analysis of variance (ANOVA) using Satterthwaite and Welch adjustments for unequal variances, respectively. RNA expression and percentages of cells by type were transformed using the natural logarithm before their analysis. When the ANOVA was significant, pairwise comparisons were evaluated using Tukey procedure. Statistical significance was reached at $P < .05$. Analyses were performed using SAS software, version 9.2 (SAS Institute, Inc, Wayne, PA).

Results

Genetic C3 Deficiency Impairs Ovarian Tumor Development and Growth

In a transplanted tumor model, we have previously characterized the spontaneous activation of complement in the tumor vasculature and stroma, as evidenced by tumor-specific deposition of the C3 cleavage products C3b/iC3b in tumor-bearing mice [16]. To determine whether complement also plays a role during early spontaneous tumor formation, we crossed $C3^{KO}$ mice with Tg*MISIIR-TAg* transgenic mice to obtain $Tg^{+}C3^{KO}$ mice. Although tumor development in the Tg*MISIIR-TAg* model is stochastic, longitudinal *in vivo* imaging and quantitative tumor growth analyses demonstrated that Tg*MISIIR-TAg* ovarian tumors are apparent by immunohistochemical staining as early as 4 weeks; ovaries exhibit enlargement by 13 weeks with a doubling time of 7.3 days [37,38], and by 16 weeks, all mice develop solid tumors that consistently reach 0.7 ± 0.2 cm^3 in volume. Tg*MISIIR-TAg* tumors are frequently accompanied by peritoneal dissemination and ascites, and the average life span of these mice is ~22 weeks [37]. Given the central role of C3 in the complement cascade, we hypothesized that $Tg^{+}C3^{KO}$ mice would be unable to generate complement effectors downstream of C3.

We compared tumor development of 16-week-old female littermates heterozygous for the TAg transgene and WT ($Tg^{+}C3^{WT}$), heterozygous ($Tg^{+}C3^{HET}$), or deficient ($Tg^{+}C3^{KO}$) for C3. All $Tg^{+}C3^{WT}$ mice developed bilateral ovarian tumors. In contrast, 9 of 12 ovaries of $Tg^{+}C3^{KO}$ mice were histologically normal (Figure 1*A*) with no visible microscopic tumors (Figure W1). In addition, tumors that developed in $Tg^{+}C3^{KO}$ and $Tg^{+}C3^{HET}$ mice were significantly smaller than $Tg^{+}C3^{WT}$ tumors (both $P \leq .001$), while $Tg^{+}C3^{KO}$ and $Tg^{+}C3^{HET}$ tumor volumes were not significantly different from each other ($P = .279$) (Figure 1*A*). $Tg^{+}C3^{KO}$ mice were unable to produce

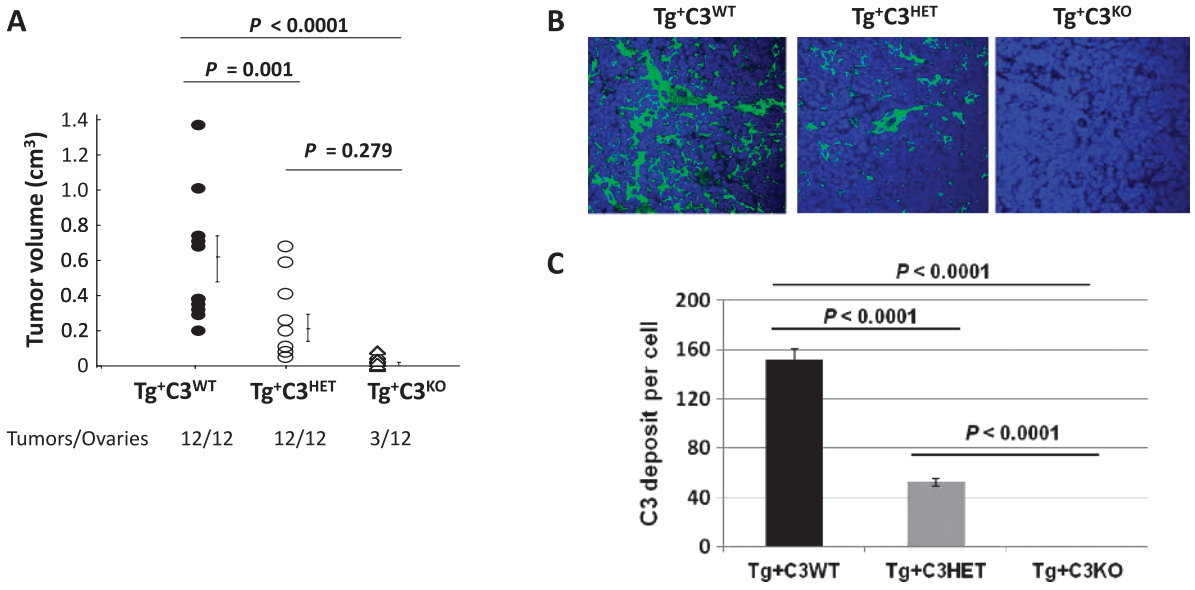

D

	SV40⁺ tumor cells (10^6)		CD45⁺ leukocytes (10^6)		SV40⁺/CD45⁺ ratios ($P = 0.355$)	
	mean	SE	mean	SE	mean	SE
$Tg^{+}C3^{WT}$	64.00	1.15	3.39	0.53	19.80	3.01
$Tg^{+}C3^{HET}$	27.40	1.80	1.47	0.62	36.55	13.59
$Tg^{+}C3^{KO}$	1.23	0.18	0.08	0.02	16.04	2.42

Figure 1. Genetic complement deficiency impairs $SV40^{+}$ ovarian tumor growth and development. (A) Tumors were collected from 16-week-old $Tg^{+}C3^{WT}$, $Tg^{+}C3^{HET}$, and $Tg^{+}C3^{KO}$ mice and measured with calipers. Volumes were calculated using the mathematical formula for the volume of an ellipsoid: $V = 4/3(3.1416)abc$, where *a*, *b*, and *c* represent the semi-axes of each diameter. $P < .05$. (B) Confocal microscopy of frozen tumor sections labeled with anti-C3b/iC3b/C3c antibody and 4′,6′-diamino-2-phenylindole (DAPI). Original magnification, ×23. Results are representative of four $Tg^{+}C3^{WT}$ tumors, four $Tg^{+}C3^{HET}$ tumors, and two $Tg^{+}C3^{KO}$ tumors. (C) Quantification of C3b/iC3b/C3c deposition on tumor cells from 16-week-old $Tg^{+}C3^{WT}$, $Tg^{+}C3^{HET}$, and $Tg^{+}C3^{KO}$ mice (*n*/group = 5). Bars represent means ± standard error. (D) Cell composition of ovarian tumors in $Tg^{+}C3^{WT}$ ($n = 3$), $Tg^{+}C3^{HET}$ ($n = 5$), and $Tg^{+}C3^{KO}$ ($n = 3$) mice by flow cytometry. Tumor cells were identified by staining with anti-SV40 Ab and tumor-infiltrating leukocytes with anti-CD45 Ab.

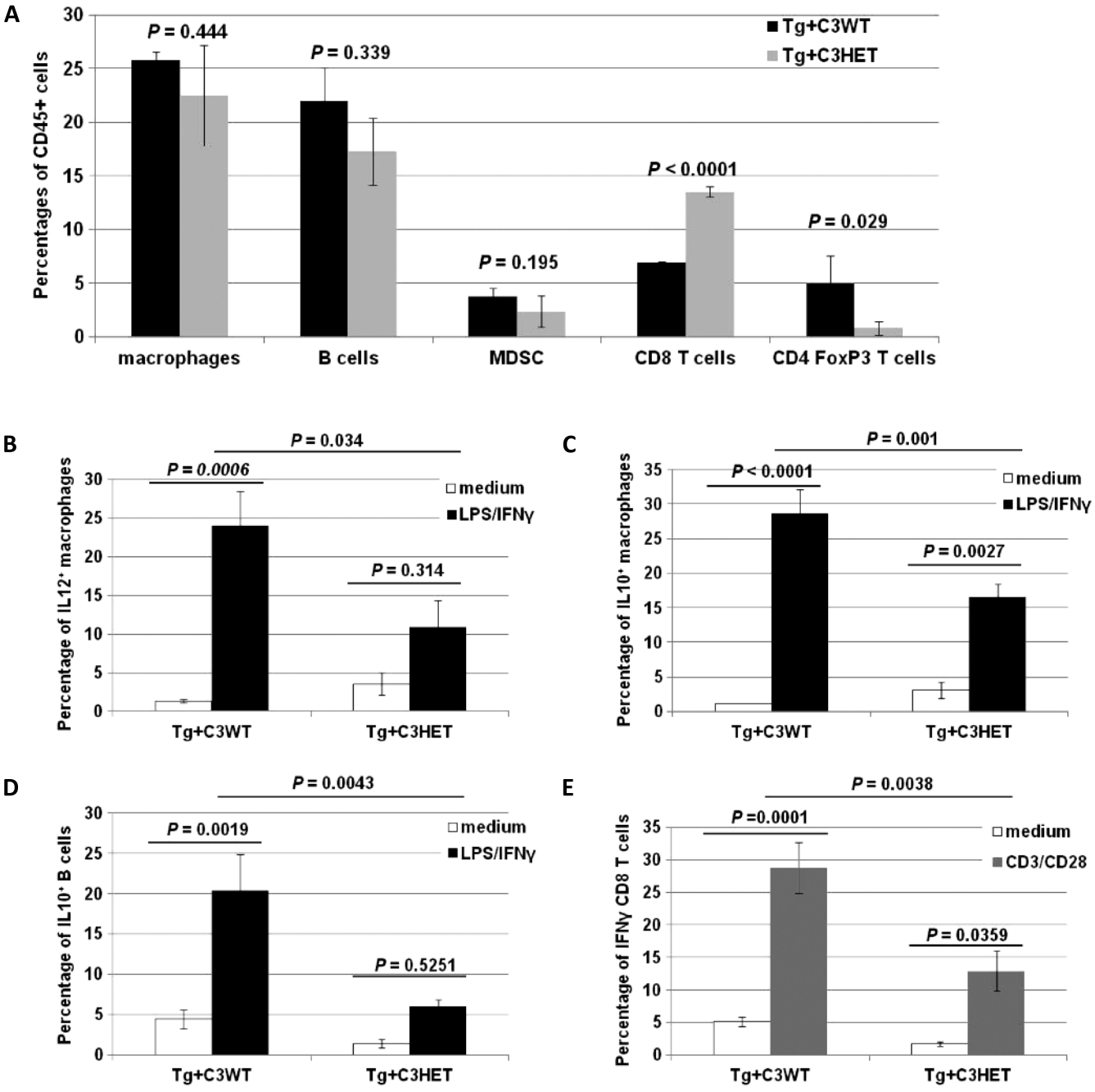

Figure 2. Functional impairment of tumor-immune infiltrate in Tg^+C3^{HET} mice. (A) Ovarian tumors from 16-week-old Tg^+C3^{WT} mice (black bars; $n = 4$) and Tg^+C3^{HET} mice (gray bars; $n = 4$) were dissociated and stained for CD45, CD11b, B220, F480, GR1, CD3, CD8, CD4, CD25, and FoxP3. $CD45^+$ leukocytes were gated and macrophages were identified as $CD11b^+F480^+$, B cells as $CD11b^-B220^+$ cells, MDSCs as $CD11b^+GR1^+$, CD8+ T cells as $CD3^+CD8^+$ cells, and regulatory T cells as $CD4^+CD25^+FoxP3^+$. Bars represent percentages of $CD45^+$ cells ± standard error. (B–E) Ovarian tumors were collected from 16-week-old Tg^+C3^{WT} ($n = 4$) and Tg^+C3^{HET} ($n = 4$) mice, mechanically dissociated to a single-cell suspension and incubated 4 hours in medium only (white bars), or activated for 4 hours with LPS and IFN-γ (black bars), or with anti-CD3 and anti-CD28 mAbs (gray bars). Cells were then stained for CD45, F480, and CD11b (macrophages) (B, C), CD45 and B220 (B cells) (D), or CD45, CD3, and CD8 (T cells) (E), washed and permeabilized for intracellular staining for IL-12 (B), IL-10 (C, D), or IFN-γ (E). Bars represent mean percentages ± standard errors.

the convertases required for the generation of complement effectors downstream of C3 because of complement deficiency, and the deposition of iC3b was attenuated in heterozygous mice (Tg^+C3^{HET}) when compared to littermates with intact complement (Tg^+C3^{WT}) (Figure 1, *B* and *C*). These results indicate that complement activation is critical for ovarian tumor establishment and growth.

C3 Deficiency Is Associated with Dampened Cellular Effector Mechanisms

The composition of tumor-infiltrating leukocytes was analyzed as a possible explanation for decreased or absent tumor growth in Tg^+C3^{HET} and Tg^+C3^{KO} mice. No difference in the percentages of tumor-infiltrating leukocytes were observed across the groups (Figure 1*D*, $P = .355$). Due

to the fact that Tg^+C3^{KO} mice bore no, or only very small, ovarian tumors with a sparse amount of tumor cell infiltrates (Figure 1*D*), we focused the rest of our studies on Tg^+C3^{WT} and Tg^+C3^{HET} tumor–infiltrating leukocytes. No significant differences in the frequency of tumor-infiltrating macrophages, B cells, and MDSCs were found between Tg^+C3^{WT} and Tg^+C3^{HET} groups at 16 weeks of age. However, Tg^+C3^{HET} tumor infiltrates contained more $CD8^+$ T cells ($P < .0001$) and less $FoxP3^+CD4^+$ T cells ($P = .029$) than Tg^+C3^{WT} tumor infiltrates (Figure 2*A*).

Macrophages and T and B cells from Tg^+C3^{HET} and Tg^+C3^{WT} littermates were then functionally characterized by flow cytometry. In the absence of stimulation (Figure 2, *B–E*, white bars), no difference were noticed among the two groups in the percentages of macrophages expressing IL-12 (Figure 2*B*, $P = .948$) or IL-10 (Figure 2*C*, $P = .447$), of B cells expressing IL-10 (Figure 2*D*, $P = .092$), or of $CD8^+$ T cells expressing IFN-γ (Figure 2*E*, $P = .765$). However, after a short stimulation with LPS and IFN-γ (Figure 2, *B–D*, black bars) or with anti-CD3 and anti-CD28 (Figure 2*E*, gray bars), the percentages of macrophages producing IL-12 (Figure 2*B*, $P = .034$) or IL-10 (Figure 2*C*, $P = .001$), of B cells producing IL-10 (Figure 2*D*, $P = .0043$), or of T cells producing IFN-γ (Figure 2*E*, $P = .0038$) were significantly lower in Tg^+C3^{HET} mice than in Tg^+C3^{WT} mice. We thus concluded that C3 deficiency was associated with dampened cellular effector mechanisms in the ovarian tumor microenvironment. This suggested that alternate mechanisms besides cell-mediated immune rejection were likely mainly responsible for the decrease in tumor incidence and growth observed in Tg^+C3^{KO} mice.

Genetic C3 Deficiency Impairs Tumor Vascularization and In Vivo *EC Function*

In preclinical models of AMD, deficiencies of C3a or C5a receptors result in decreased choroidal neovascularization and VEGF levels. Similar observations were reported when WT mice were treated with C3aR and C5aR antagonists, or neutralizing antibodies against C3a and C5a [21], suggesting an important role for complement in modulating vascularization. In humans, the number of chronically activated tumor-infiltrating innate immune cells is positively correlated with blood vessel density [54], while the attenuation of innate immunity in premalignant tissues reduces angiogenesis and limits tumor development in murine models [55]. We therefore asked whether defective angiogenesis was responsible for the reduced tumor formation in our model. Tumor microvascular density (MVD) was assessed by CD31 staining and quantification of vessel number in Tg^+C3^{HET} and Tg^+C3^{WT} littermates. MVD was significantly decreased in tumors from Tg^+C3^{HET} littermates (Figure 3*A*, $P = .023$), suggesting a functional role of complement for ECs. To address whether genetic

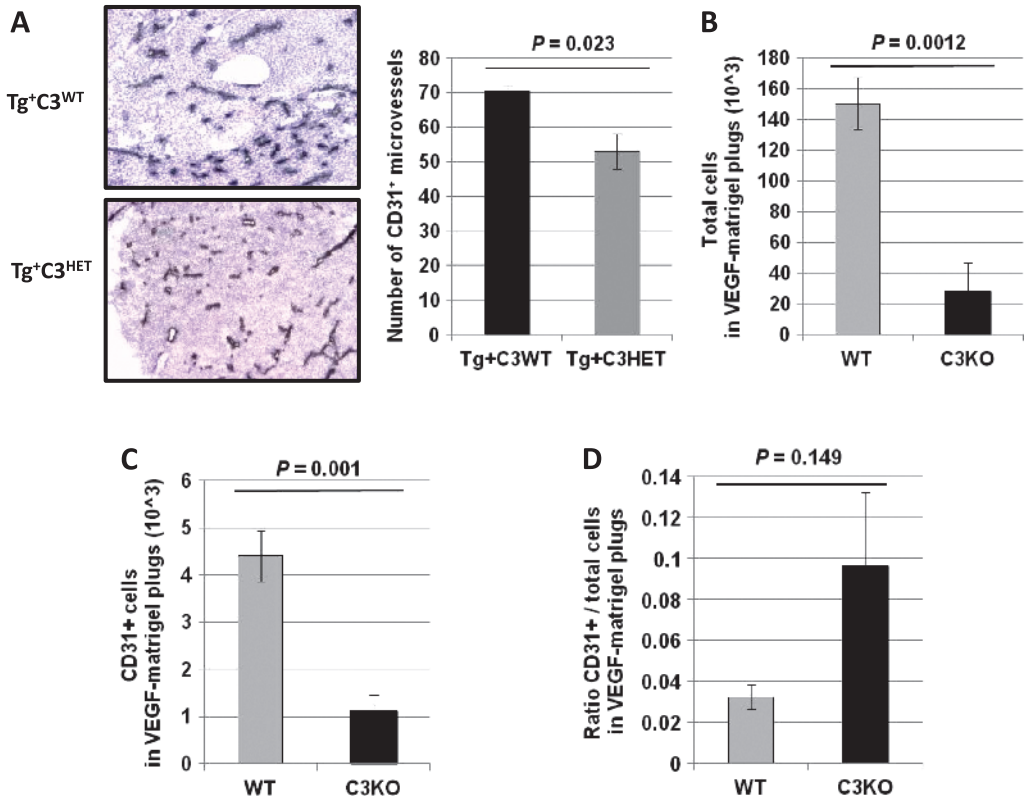

Figure 3. Genetic complement deficiency impairs neo-angiogenesis. (A) Tumor microvasculature was evaluated by CD31 staining (dark blue staining) of frozen tumor sections from 16-week-old Tg^+C3^{WT} and Tg^+C3^{HET} mice. Values reflect the number of $CD31^+$ vessels averaged from five high-power fields per slide per mouse. Original magnification, ×10. Bars represent means of $CD31^+$ microvessels ± standard error. (B–D) Bars represent the absolute number of total cells (B), or $CD31^+$ ECs (C), or the ratios of $CD31^+$ ECs and total cells (D) attracted to Matrigel plugs admixed with recombinant VEGF (10 ng/ml) and implanted in C57BL/6 mice (WT, gray bar, *n*/group = 5) or $C3^{KO}$ mice (black bar, *n*/group = 5) ± standard error.

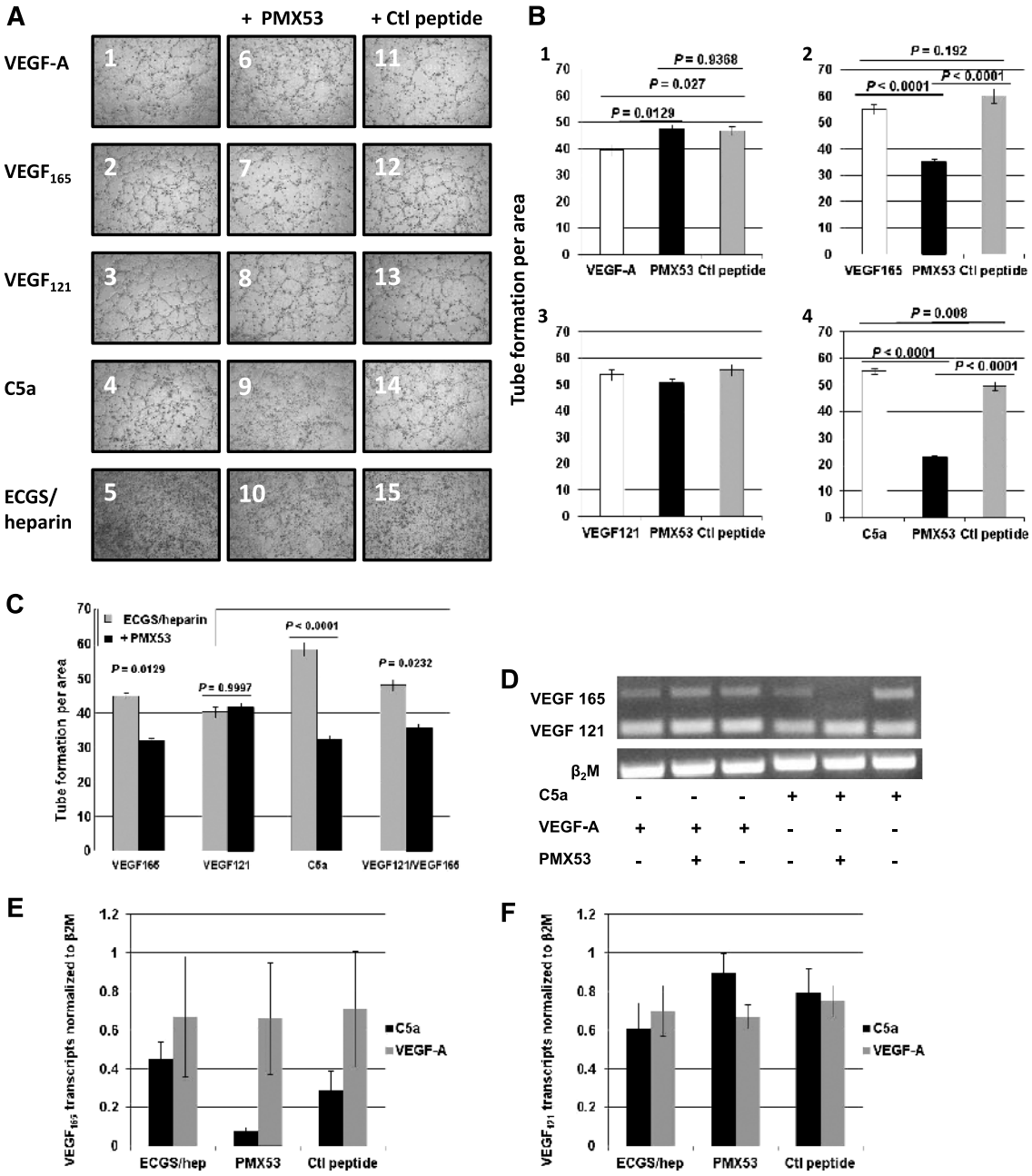

Figure 4. Pharmacological inhibition of C5aR targets the $VEGF_{165}$ isoform. (A) Representative pictures of tube formation. Human microvascular ECs (2×10^5) were seeded onto Matrigel and cultured in MCDB-131 culture medium supplemented with ECGS/heparin and 2 ng/ml of either VEGF-A (1, 6, 11), $VEGF_{165}$ (2, 7, 12), or $VEGF_{121}$ (3, 8, 13), or 2 nM C5a (4, 9, 14) in the presence of 200 ng/ml PMX53 (6–10) or PMX53 control peptide (Ctl peptide, 11–15). As negative controls, cells were cultured with medium supplemented with ECGS/heparin only (5, 10, 15). Tube formation was assayed after 4 hours by phase contrast microscopy and analyzed by measuring tube length per area using the ImagePro software. (B, C) Measures of tube formation of four fields per treatment (B) with 2 ng/ml VEGF-A, $VEGF_{165}$, or $VEGF_{121}$ or (C) with equimolar concentrations of $VEGF_{165}$ (2.7 ng/ml) and/or $VEGF_{121}$ (2 ng/ml). Bars represent means ± standard error from two independent experiments. (D) Representative picture of PCR amplification of VEGF isoform in the presence or absence of C5a, VEGF-A, and/or PMX53 (as indicated). PCR amplification of β_2-microglobulin was used as a control. (E, F) Densitometric analysis of transcript expression of $VEFG_{165}$ (E) and $VEFG_{121}$ (F) isoforms in HMECs treated with 2 nM C5a (black bars) or 2 ng/ml VEGF-A (gray bars) in medium or in the presence of 200 ng/ml PMX53 or control peptide (as indicated). VEGF isoform values were normalized to those of β_2-microglobulin. Bars represent mean ± standard error from five independent experiments.

complement deficiency could alter *in vivo* angiogenesis, we compared the *in vivo* colonization of Matrigel plugs admixed with VEGF in WT and $C3^{KO}$ mice. The numbers of total cells infiltrating VEGF–Matrigel plugs after 2 weeks were significantly reduced in $C3^{KO}$ mice compared to WT mice (Figure 3*B*, $P = .0012$), as was the number of $CD31^+$ ECs (Figure 3*C*, $P < .0001$). However, the ratios of $CD31^+$ ECs *versus* total cells were not significantly different in WT and $C3^{KO}$ mouse VEGF–Matrigel plugs (Figure 3*D*, $P = .149$). These results

supported the hypothesis that genetic C3 heterogeneity or deficiency impairs EC effector mechanisms in our model.

Pharmacological Inhibition of Complement Impairs $VEGF_{165}$-dependent Function of Human ECs

To assess whether our *in vivo* findings were relevant to human physiology, we sought to study the effects of complement pharmacological inhibition on the human EC line HMEC. The C5aR is expressed on ECs and upregulated during inflammation [56,57]. C5aR function can be inhibited by PMX53, a peptide that has been used in preclinical models to block neutrophil chemotaxis and clinically for treatment of rheumatoid arthritis and psoriasis [58]. We studied the effects of PMX53-mediated inhibition of C5aR on HMEC tube formation stimulated by VEGF-A (Figure 4, *A1* and *B1*, white bar) and the commercially available isoforms $VEGF_{165}$ (Figure 4, *A2* and *B2*, white bar) and $VEGF_{121}$ (Figure 4, *A3* and *B3*, white bar) compared to a control peptide (Figure 4, *A11–15* and *B*, gray bars). PMX53 (Figure 4*B*, black bars) impaired $VEGF_{165}$-mediated tube formation (Figure 4, *A7*, *B2*, and *C*) but not $VEGF_{121}$-mediated tube formation (Figure 4, *A8*, *B3*, and *C*, ANOVA $P > .05$). PMX53 also impaired HMEC tube formation mediated by equimolar concentrations of $VEGF_{165}$ and $VEGF_{121}$ (Figure 4*C*, $P = .0232$). As expected, treatment with control peptide did not affect tube formation. Of note, the difference observed between ECs activated by VEGF-A and treated with PMX53 was statistically significant but not meaningful (Figure 4, *A6* and *B1*, $P = .0127$ for VEGF-A *vs* VEGF-A/PMX53 but $P = .9368$ for VEGF-A/PMX53 *vs* VEGF-A/control peptide). These results suggested that C5aR inhibition selectively affected tube formation mediated by the $VEGF_{165}$ isoform.

C5a Promotes Tube Formation in a $VEGF_{165}$-dependent Manner

To determine whether C5a had direct functional effects on ECs, HMECs were incubated with native C5a protein at 2 nM (20.8 ng/ml), which is within the plasma concentration range of C5a degradation product C5adesArg [59]. Tube formation similar to that mediated by VEGF-A and VEGF isoforms was observed (Figure 4, *A4* and *B4*, white bar), while PMX53 inhibited C5a-mediated tube formation (Figure 4, *A9* and *B4*, black bar, $P < .0001$). In addition, we found that PMX53 specifically inhibited the transcription of $VEGF_{165}$ (Figure 4, *D–E*, $P = .050$) but not of $VEGF_{121}$ in C5a-treated HMEC cells (Figure 4, *D* and *F*, $P = .202$). These results suggested a novel role for C5a in promoting EC tube formation through enhancing expression of $VEGF_{165}$.

Genetic C3 Deficiency Affects the Expression of $VEGF_{164}$ Isoform

As experimental evidence pointed toward a role for C5a in $VEGF_{165}$-mediated activation of human ECs, we performed a comparative analysis of the expression of VEGF isoforms in mice that are complement deficient or complement sufficient. We analyzed the expression of the mouse homologues of human $VEGF_{121}$ and $VEGF_{165}$ that are mouse isoforms $VEGF_{120}$ and $VEGF_{164}$, respectively, in the spleens, livers, and bone marrows isolated from WT and $C3^{KO}$ mice. Figure 5 represents the relative expression of VEGF isoforms in WT and $C3^{KO}$ mice after normalization against GAPDH. The expression of $VEGF_{164}$, but not of VEGF120, was significantly reduced in $C3^{KO}$ livers compared to WT livers (Figure 5*A*, $P = .048$ and Figure 5*B*, $P = .404$).

Genetic C5aR Deficiency Impairs Tumor Growth and Neo-angiogenesis but Not Tumor Immune Infiltrate

To further assess the role of the C5a complement anaphylatoxin in ovarian cancer progression and angiogenesis, we crossed $C5aR^{KO}$ mice [35] with C57BL/6 Tg*MISIIR-TAg* transgenic mice. We compared tumor development in 16-week-old female littermates heterozygous for the TAg transgene and C5aR sufficient (Tg^+C5aR^{WT}), C5aR heterozygous (Tg^+C5aR^{HET}), or C5aR deficient (Tg^+C5aR^{KO}). While Tg^+C5aR^{WT} and Tg^+C5aR^{HET} mice developed unilateral ovarian tumors, three of six ovaries of Tg^+C5aR^{KO} mice were histologically normal and Tg^+C5aR^{KO} tumors were significantly smaller than Tg^+C5aR^{WT} and Tg^+C5aR^{HET} tumors (Figure 6*A*, $P = .001$ and $P = .002$, respectively). In contrast with *C3* deficiency, no difference in tumor sizes was observed between Tg^+C5aR^{WT} and Tg^+C5aR^{HET} mice (Figure 6*A*, $P = .945$), and no significant differences were found across the groups regarding tumor immune infiltrate (Figure 6*B*, all ANOVA $P > .05$). However, as seen in Tg^+C3^{HET} mice, tumor MVD was significantly decreased in tumors from Tg^+C5aR^{HET} mice as well as Tg^+C5aR^{KO} mice compared to Tg^+C5aR^{WT} littermates (Figure 6*C*, $P = .0004$ and $P < .0001$, respectively). Additionally, MVD in tumors from Tg^+C5aR^{KO} mice was significantly decreased compared to Tg^+C5aR^{HET} mice (Figure 6*C*, $P < .0001$). Finally, *in vivo* assays showed significantly impaired angiogenesis in $C5aR^{KO}$ mice compared to WT mice (Figure 6*D*, $P = .019$). Collectively, these results supported the hypothesis that the tumor growth inhibition observed in mice with

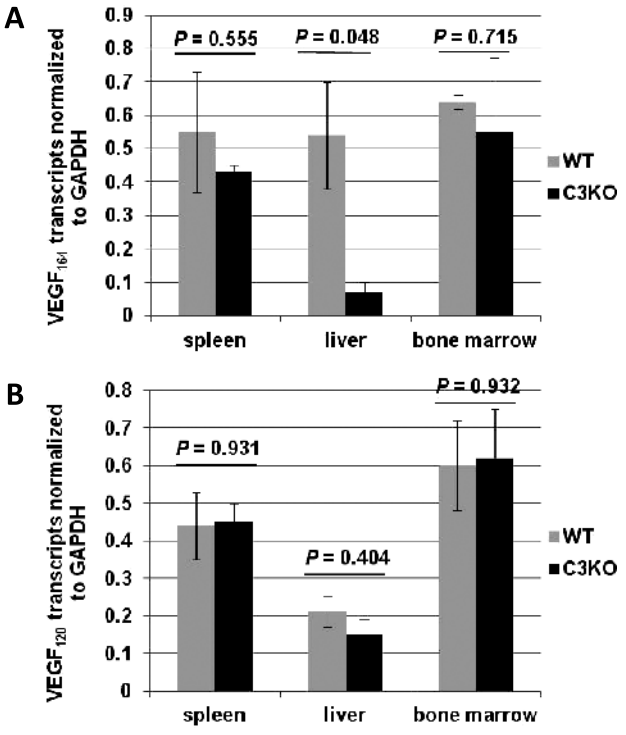

Figure 5. Altered expression of $VEGF_{164}$ isoform in complement-deficient mice. Densitometry analysis of expression of mouse $VEFG_{164}$ (A) and $VEFG_{120}$ (B) isoforms in WT *versus* $C3^{KO}$ spleens, livers, and bone marrows (as indicated). VEGF isoform values were normalized to those of GAPDH. Bars display mean ± standard error from three different mice per group.

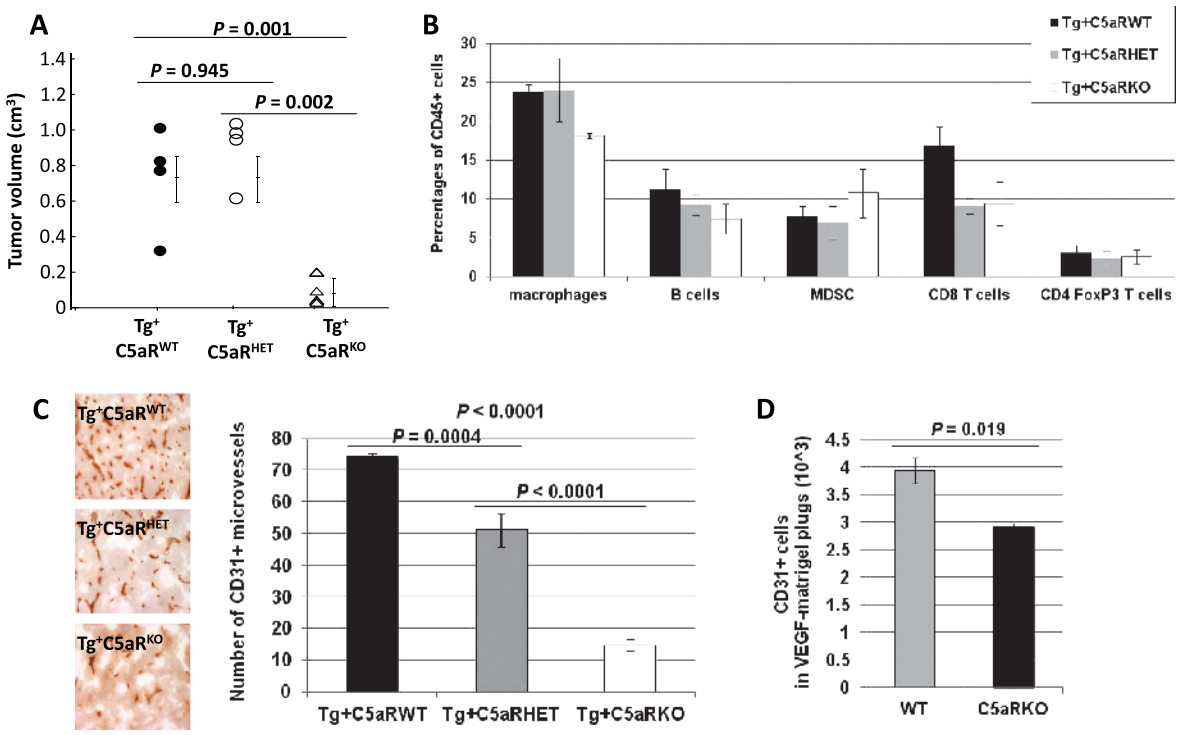

Figure 6. Genetic C5aR deficiency also impairs ovarian cancer growth and vascularization but not tumor immune infiltrate. (A) Tumors were collected from 16-week-old Tg^+C5aR^{WT} ($n = 4$), Tg^+C5aR^{HET} ($n = 4$), and Tg^+C5aR^{KO} mice ($n = 3$) and measured with calipers. Volumes were calculated using the mathematical formula for the volume of an ellipsoid: $V = 4/3(3.1416)abc$, where a, b, and c represent the semi-axes of each diameter. (B) Comparative composition of tumor-infiltrating leukocyte function in Tg^+C5aR^{WT}, Tg^+C5aR^{HET}, and Tg^+C5aR^{KO} mice. Ovarian tumors from 16-week-old Tg^+C5aR^{WT} mice (black bars, $n = 3$), Tg^+C5aR^{HET} mice (gray bars, $n = 3$), and Tg^+C5aR^{KO} mice (white bars, $n = 3$) were dissociated and stained as described in Figure 2*A*. Bars represent mean percentages ± standard errors. (C) Tumor microvasculature was evaluated by CD31 staining and immunohistochemistry (IHC) (dark brown staining) of tumors from 16-week-old Tg^+C5aR^{WT}, Tg^+C5aR^{HET}, and Tg^+C5aR^{KO} mice. Values reflect the number of $CD31^+$ vessels averaged from five high-power fields per slide per mouse. Original magnification, ×10. Bars represent means of $CD31^+$ microvessels ± standard errors from at least four tumors per group. (D) Bars represent $CD31^+$ ECs attracted to Matrigel plugs admixed with VEGF (10 ng/ml) in C57BL/6 mice (WT) (n/group = 5) or $C5aR^{KO}$ mice (n/group = 5) ± standard error.

genetic complement deficiencies was associated with the alteration of EC function.

Discussion

Cancer establishment and progression is a multistep process of cumulative genetic alterations that enable cells to acquire uncontrolled growth. It has recently become clear, however, that to initiate cancer growth, genetically induced cell autonomy is often not sufficient, and an inflammatory reaction of the underlying stroma is required. The idea that chronic inflammation is intimately related to malignant transformation and tumor progression has been substantiated by human epidemiologic data and genetic experiments in mice, but the molecular and cellular determinants of these processes have not been well characterized. Here, we showed that deficiency of *C3* or *C5aR* dramatically attenuates the tumor phenotype, abrogating tumor establishment and progression. Thus, complement activation is a critical component of the inflammatory process that supports oncogene-driven carcinogenesis. However, complement inactivation did not reduce the inflammatory infiltrate in tumors; we found no difference in the percentage of tumor-infiltrating leukocytes in Tg^+C3^{HET} when compared to Tg^+C3^{WT}, with the exception of $CD8^+$ T cells and $CD4^+$ $FoxP3^+$ T cells. This suggests that, contrary to the acute inflammation process in which complement anaphylatoxins likely play a major role in orchestrating the inflammatory infiltrate, other factors, such as chemokines produced by tumor and stromal cells, recruit copious amounts of leukocytes to tumors, even in the absence of complement activation. The presence of more tumor-infiltrating effector T cells and less regulatory T cells in Tg^+C3^{HET} compared to Tg^+C3^{WT} was in agreement with our previous findings in a mouse model of subcutaneous TC-1 cervical cancer, in which impaired growth of tumor cells was found when C5aR was blocked by an antagonist peptide [16]; this effect was attributed to enhanced $CD8^+$ T-cell infiltration in tumors and reduced recruitment of MDSCs [16]. Furthermore, we found no evidence for immune cell activation in Tg^+C3^{HET} tumors but rather a general suppression of leukocyte function, including a global reduction of cytokine production in Tg^+C3^{HET} mice when compared to those fully sufficient in C3. These findings thus showed only indirect evidence of immune-mediated tumor rejection in these mice, through the decrease of immune regulatory cells or cytokines. Likewise, no evidence of immune-mediated tumor rejection was found in C5aR-hemizygous or C5aR-deficient mice, despite the dramatic attenuation of the tumor phenotype. The lower percentage of tumor-infiltrating $CD4^+FoxP3^+$ T cells in Tg^+C3^{HET} tumors could explain why the Tg^+C3^{HET} mice, but not the Tg^+C5aR^{HET} mice, developed smaller tumors than their WT littermates. However, this finding was

not sufficient to explain the dramatic phenotype of Tg^+C5aR^{KO} mice where no change in tumor-infiltrating $CD4^+FoxP3^+$ T cells was found. Thus, while our data support the notion that complement activation plays a critical role in activating tumor-infiltrating leukocytes, a process that is apparently essential to their tumor-promoting function, our data also indicate that increased activation of effector cells is not the major mechanism leading to suppressed ovarian oncogenesis in C3-hemizygous and C5aR-hemizygous or C5aR-deficient mice, and there is likely an alternate mechanism of tumor inhibition.

Because tumor-induced angiogenesis is largely dependent on VEGF, VEGF-neutralizing drugs are actively sought to inhibit cancer growth. Current VEGF-neutralizing agents inhibit tumor angiogenesis by blocking activation of VEGF receptors [60], but agents have already been developed to selectively target VEGF isoforms. For example, Pegaptanib targets $VEGF_{165}$ for the treatment of AMD [61], and the specific targeting of VEGF isoforms has been proposed as an effective cancer therapy [62]. We show here that the complement anaphylatoxin C5a present in the inflammatory milieu activates ECs and that the pharmacological inhibition of C5aR specifically targets the $VEGF_{165}$ isoform. Our results reveal a previously unknown role for complement activation in ovarian tumor vascularization and growth. However, these data should be considered within the context of our ovarian tumor model. While another study has shown that lack of C3 results in increased angiogenesis in a model of retinopathy of prematurity [63], here it was found that C5a stimulation of ECs mediates angiogenic activity. Thus, the specific pathology may determine how complement influences different cell types, as well as the outcomes of that influence. The fact that small, unilateral ovarian tumors were present in 3 of 12 Tg^+C3^{KO} mouse ovaries might be due to phenotype variability or incomplete penetrance not related to variations in genetic background or levels in gene expression [64,65]. Because $C3^{KO}$ mice produce C3 transcript and some of it can be translated into an inactive pro-form of C3 protein, one cannot eliminate the possibility that some active C3 can be produced in the Tg^+C3^{KO} mice through alternate splicing or processing. Alternatively, some unrelated factors could have also been differentially activated in these mice, such as the tumor microenvironment, or a different microbiome that could affect factors related to tumor growth, or even epigenetics. Future studies are needed to determine the molecular mechanisms underlying Tg^+C3^{KO} phenotype variability.

In conclusion, our findings have important implications for our understanding of the mechanisms underlying ovarian cancer development and for the design of future preventive and therapeutic strategies, such as combination therapies associating complement inhibitors with targeted anti-angiogenic therapeutic agents for the treatment of ovarian cancer.

References

[1] Coussens LM and Werb Z (2002). Inflammation and cancer. *Nature* **420**, 860–867.

[2] Balkwill F and Mantovani A (2001). Inflammation and cancer: back to Virchow? *Lancet* **357**, 539–545.

[3] Thun MJ, Henley SJ, and Patrono C (2002). Nonsteroidal anti-inflammatory drugs as anticancer agents: mechanistic, pharmacologic, and clinical issues. *J Natl Cancer Inst* **94**, 252–266.

[4] Cipriano C, Giacconi R, Muzzioli M, Gasparini N, Orlando F, Corradi A, Cabassi E, and Mocchegiani E (2003). Metallothionein (I+II) confers, via *c-myc*, immune plasticity in oldest mice: model of partial hepatectomy/liver regeneration. *Mech Ageing Dev* **124**, 877–886.

[5] Cuzick J, Otto F, Baron JA, Brown PH, Burn J, Greenwald P, Jankowski J, La Vecchia C, Meyskens F, Senn HJ, et al. (2009). Aspirin and non-steroidal anti-inflammatory drugs for cancer prevention: an international consensus statement. *Lancet Oncol* **10**, 501–507.

[6] Ness RB, Goodman MT, Shen C, and Brunham RC (2003). Serologic evidence of past infection with *Chlamydia trachomatis*, in relation to ovarian cancer. *J Infect Dis* **187**, 1147–1152.

[7] Merritt MA, Green AC, Nagle CM, and Webb PM (2008). Talcum powder, chronic pelvic inflammation and NSAIDs in relation to risk of epithelial ovarian cancer. *Int J Cancer* **122**, 170–176.

[8] Gorelik E, Landsittel DP, Marrangoni AM, Modugno F, Velikokhatnaya L, Winans MT, Bigbee WL, Herberman RB, and Lokshin AE (2005). Multiplexed immunobead-based cytokine profiling for early detection of ovarian cancer. *Cancer Epidemiol Biomarkers Prev* **14**, 981–987.

[9] Auersperg N, Wong AS, Choi KC, Kang SK, and Leung PC (2001). Ovarian surface epithelium: biology, endocrinology, and pathology. *Endocr Rev* **22**, 255–288.

[10] Knutson KL, Curiel TJ, Salazar L, and Disis ML (2003). Immunologic principles and immunotherapeutic approaches in ovarian cancer. *Hematol Oncol Clin North Am* **17**, 1051–1073.

[11] Kulbe H, Hagemann T, Szlosarek PW, Balkwill FR, and Wilson JL (2005). The inflammatory cytokine tumor necrosis factor-alpha regulates chemokine receptor expression on ovarian cancer cells. *Cancer Res* **65**, 10355–10362.

[12] Bjorge L, Hakulinen J, Vintermyr OK, Jarva H, Jensen TS, Iversen OE, and Meri S (2005). Ascitic complement system in ovarian cancer. *Br J Cancer* **92**, 895–905.

[13] Markiewski MM and Lambris JD (2007). The role of complement in inflammatory diseases from behind the scenes into the spotlight. *Am J Pathol* **171**, 715–727.

[14] Ricklin D, Hajishengallis G, Yang K, and Lambris JD (2010). Complement: a key system for immune surveillance and homeostasis. *Nat Immunol* **11**, 785–797.

[15] Oikonomopoulou K, Ricklin D, Ward PA, and Lambris JD (2012). Interactions between coagulation and complement—their role in inflammation. *Semin Immunopathol* **34**, 151–165.

[16] Markiewski MM, DeAngelis RA, Benencia F, Ricklin-Lichtsteiner SK, Koutoulaki A, Gerard C, Coukos G, and Lambris JD (2008). Modulation of the antitumor immune response by complement. *Nat Immunol* **9**, 1225–1235.

[17] Cortright DN, Meade R, Waters SM, Chenard BL, and Krause JE (2009). C5a, but not C3a, increases VEGF secretion in ARPE-19 human retinal pigment epithelial cells. *Curr Eye Res* **34**, 57–61.

[18] Yanai R, Thanos A, and Connor KM (2012). Complement involvement in neovascular ocular diseases. *Adv Exp Med Biol* **946**, 161–183.

[19] Girardi G, Yarilin D, Thurman JM, Holers VM, and Salmon JE (2006). Complement activation induces dysregulation of angiogenic factors and causes fetal rejection and growth restriction. *J Exp Med* **203**, 2165–2175.

[20] Lynch AM and Salmon JE (2010). Dysregulated complement activation as a common pathway of injury in preeclampsia and other pregnancy complications. *Placenta* **31**, 561–567.

[21] Nozaki M, Raisler BJ, Sakurai E, Sarma JV, Barnum SR, Lambris JD, Chen Y, Zhang K, Ambati BK, Baffi JZ, et al. (2006). Drusen complement components C3a and C5a promote choroidal neovascularization. *Proc Natl Acad Sci USA* **103**, 2328–2333.

[22] van der Bilt AR, de Vries EG, de Jong S, Timmer-Bosscha H, van der Zee AG, and Reyners AK (2012). Turning promise into progress for antiangiogenic agents in epithelial ovarian cancer. *Crit Rev Oncol Hematol*, E-pub ahead of print April 21.

[23] Mattei MG, Borg JP, Rosnet O, Marme D, and Birnbaum D (1996). Assignment of vascular endothelial growth factor (VEGF) and placenta growth factor (PLGF) genes to human chromosome 6p12-p21 and 14q24-q31 regions, respectively. *Genomics* **32**, 168–169.

[24] Roskoski R Jr (2007). Vascular endothelial growth factor (VEGF) signaling in tumor progression. *Crit Rev Oncol Hematol* **62**, 179–213.

[25] Tischer E, Mitchell R, Hartman T, Silva M, Gospodarowicz D, Fiddes JC, and Abraham JA (1991). The human gene for vascular endothelial growth factor. Multiple protein forms are encoded through alternative exon splicing. *J Biol Chem* **266**, 11947–11954.

[26] Grunstein J, Masbad JJ, Hickey R, Giordano F, and Johnson RS (2000). Isoforms of vascular endothelial growth factor act in a coordinate fashion to recruit and expand tumor vasculature. *Mol Cell Biol* **20**, 7282–7291.

[27] Ferrara N (2000). Vascular endothelial growth factor and the regulation of angiogenesis. *Recent Prog Horm Res* **55**, 15–35; discussion 35-16.

[28] Cheng SY, Nagane M, Huang HS, and Cavenee WK (1997). Intracerebral tumor-associated hemorrhage caused by overexpression of the vascular endothelial growth factor isoforms VEGF121 and VEGF165 but not VEGF189. *Proc Natl Acad Sci USA* **94**, 12081–12087.

[29] Zhang HT, Scott PA, Morbidelli L, Peak S, Moore J, Turley H, Harris AL, Ziche M, and Bicknell R (2000). The 121 amino acid isoform of vascular endothelial growth factor is more strongly tumorigenic than other splice variants *in vivo*. *Br J Cancer* **83**, 63–68.

[30] Tokunaga T, Oshika Y, Abe Y, Ozeki Y, Sadahiro S, Kijima H, Tsuchida T, Yamazaki H, Ueyama Y, Tamaoki N, et al. (1998). Vascular endothelial growth factor (VEGF) mRNA isoform expression pattern is correlated with liver metastasis and poor prognosis in colon cancer. *Br J Cancer* **77**, 998–1002.

[31] Yuan A, Yu CJ, Kuo SH, Chen WJ, Lin FY, Luh KT, Yang PC, and Lee YC (2001). Vascular endothelial growth factor 189 mRNA isoform expression specifically correlates with tumor angiogenesis, patient survival, and postoperative relapse in non–small-cell lung cancer. *J Clin Oncol* **19**, 432–441.

[32] Mahner S, Woelber L, Eulenburg C, Schwarz J, Carney W, Jaenicke F, Milde-Langosch K, and Mueller V (2010). TIMP-1 and VEGF-165 serum concentration during first-line therapy of ovarian cancer patients. *BMC Cancer* **10**, 139.

[33] Perren TJ, Swart AM, Pfisterer J, Ledermann JA, Pujade-Lauraine E, Kristensen G, Carey MS, Beale P, Cervantes A, Kurzeder C, et al. (2011). A phase 3 trial of bevacizumab in ovarian cancer. *N Engl J Med* **365**, 2484–2496.

[34] Circolo A, Garnier G, Fukuda W, Wang X, Hidvegi T, Szalai AJ, Briles DE, Volanakis JE, Wetsel RA, and Colten HR (1999). Genetic disruption of the murine complement C3 promoter region generates deficient mice with extrahepatic expression of C3 mRNA. *Immunopharmacology* **42**, 135–149.

[35] Hopken UE, Lu B, Gerard NP, and Gerard C (1996). The C5a chemoattractant receptor mediates mucosal defence to infection. *Nature* **383**, 86–89.

[36] Connolly DC, Bao R, Nikitin AY, Stephens KC, Poole TW, Hua X, Harris SS, Vanderhyden BC, and Hamilton TC (2003). Female mice chimeric for expression of the simian virus 40 TAg under control of the MISIIR promoter develop epithelial ovarian cancer. *Cancer Res* **63**, 1389–1397.

[37] Hensley H, Quinn BA, Wolf RL, Litwin SL, Mabuchi S, Williams SJ, Williams C, Hamilton TC, and Connolly DC (2007). Magnetic resonance imaging for detection and determination of tumor volume in a genetically engineered mouse model of ovarian cancer. *Cancer Biol Ther* **6**, 1717–1725.

[38] Quinn BA, Xiao F, Bickel L, Martin L, Hua X, Klein-Szanto A, and Connolly DC (2010). Development of a syngeneic mouse model of epithelial ovarian cancer. *J Ovarian Res* **3**, 24.

[39] Greenberg NM, DeMayo F, Finegold MJ, Medina D, Tilley WD, Aspinall JO, Cunha GR, Donjacour AA, Matusik RJ, and Rosen JM (1995). Prostate cancer in a transgenic mouse. *Proc Natl Acad Sci USA* **92**, 3439–3443.

[40] Hanahan D (1985). Heritable formation of pancreatic beta-cell tumours in transgenic mice expressing recombinant insulin/simian virus 40 oncogenes. *Nature* **315**, 115–122.

[41] Grippo PJ and Sandgren EP (2000). Highly invasive transitional cell carcinoma of the bladder in a simian virus 40 T-antigen transgenic mouse model. *Am J Pathol* **157**, 805–813.

[42] Chailley-Heu B, Rambaud C, Barlier-Mur AM, Galateau-Salle F, Perret C, Capron F, and Lacaze-Masmonteil T (2001). A model of pulmonary adenocarcinoma in transgenic mice expressing the simian virus 40 T antigen driven by the rat Calbindin-D9K (CaBP9K) promoter. *J Pathol* **195**, 482–489.

[43] Bergers G, Javaherian K, Lo KM, Folkman J, and Hanahan D (1999). Effects of angiogenesis inhibitors on multistage carcinogenesis in mice. *Science* **284**, 808–812.

[44] Casanovas O, Hicklin DJ, Bergers G, and Hanahan D (2005). Drug resistance by evasion of antiangiogenic targeting of VEGF signaling in late-stage pancreatic islet tumors. *Cancer Cell* **8**, 299–309.

[45] Nozawa H, Chiu C, and Hanahan D (2006). Infiltrating neutrophils mediate the initial angiogenic switch in a mouse model of multistage carcinogenesis. *Proc Natl Acad Sci USA* **103**, 12493–12498.

[46] Du YC, Lewis BC, Hanahan D, and Varmus H (2007). Assessing tumor progression factors by somatic gene transfer into a mouse model: Bcl-xL promotes islet tumor cell invasion. *PLoS Biol* **5**, e276.

[47] Aunoble B, Sanches R, Didier E, and Bignon YJ (2000). Major oncogenes and tumor suppressor genes involved in epithelial ovarian cancer (review). *Int J Oncol* **16**, 567–576.

[48] Feeley KM and Wells M (2001). Precursor lesions of ovarian epithelial malignancy. *Histopathology* **38**, 87–95.

[49] Dodson MK, Cliby WA, Xu HJ, DeLacey KA, Hu SX, Keeney GL, Li J, Podratz KC, Jenkins RB, and Benedict WF (1994). Evidence of functional RB protein in epithelial ovarian carcinomas despite loss of heterozygosity at the RB locus. *Cancer Res* **54**, 610–613.

[50] Hashiguchi Y, Tsuda H, Yamamoto K, Inoue T, Ishiko O, and Ogita S (2001). Combined analysis of p53 and RB pathways in epithelial ovarian cancer. *Hum Pathol* **32**, 988–996.

[51] Chow WN, Lee YL, Wong PC, Chung MK, Lee KF, and Yeung WS (2009). Complement 3 deficiency impairs early pregnancy in mice. *Mol Reprod Dev* **76**, 647–655.

[52] Facciabene A, Peng X, Hagemann IS, Balint K, Barchetti A, Wang LP, Gimotty PA, Gilks CB, Lal P, Zhang L, et al. (2011). Tumour hypoxia promotes tolerance and angiogenesis via CCL28 and T(reg) cells. *Nature* **475**, 226–230.

[53] Medford AR, Douglas SK, Godinho SI, Uppington KM, Armstrong L, Gillespie KM, van Zyl B, Tetley TD, Ibrahim NB, and Millar AB (2009). Vascular endothelial growth factor (VEGF) isoform expression and activity in human and murine lung injury. *Respir Res* **10**, 27.

[54] Esposito I, Menicagli M, Funel N, Bergmann F, Boggi U, Mosca F, Bevilacqua G, and Campani D (2004). Inflammatory cells contribute to the generation of an angiogenic phenotype in pancreatic ductal adenocarcinoma. *J Clin Pathol* **57**, 630–636.

[55] de Visser KE, Korets LV, and Coussens LM (2005). *De novo* carcinogenesis promoted by chronic inflammation is B lymphocyte dependent. *Cancer Cell* **7**, 411–423.

[56] Wetsel RA (1995). Expression of the complement C5a anaphylatoxin receptor (C5aR) on non-myeloid cells. *Immunol Lett* **44**, 183–187.

[57] Gasque P, Singhrao SK, Neal JW, Gotze O, and Morgan BP (1997). Expression of the receptor for complement C5a (CD88) is up-regulated on reactive astrocytes, microglia, and endothelial cells in the inflamed human central nervous system. *Am J Pathol* **150**, 31–41.

[58] Qu H, Magotti P, Ricklin D, Wu EL, Kourtzelis I, Wu YQ, Kaznessis YN, and Lambris JD (2010). Novel analogues of the therapeutic complement inhibitor compstatin with significantly improved affinity and potency. *Mol Immunol* **48**, 481–489.

[59] Stove S, Welte T, Wagner TO, Kola A, Klos A, Bautsch W, and Kohl J (1996). Circulating complement proteins in patients with sepsis or systemic inflammatory response syndrome. *Clin Diagn Lab Immunol* **3**, 175–183.

[60] Eatock MM, Schatzlein A, and Kaye SB (2000). Tumour vasculature as a target for anticancer therapy. *Cancer Treat Rev* **26**, 191–204.

[61] Gragoudas ES, Adamis AP, Cunningham ET Jr, Feinsod M, and Guyer DR (2004). Pegaptanib for neovascular age-related macular degeneration. *N Engl J Med* **351**, 2805–2816.

[62] Finley SD and Popel AS (2012). Predicting the effects of anti-angiogenic agents targeting specific VEGF isoforms. *AAPS J* **14**, 500–509.

[63] Langer HF, Chung KJ, Orlova VV, Choi EY, Kaul S, Kruhlak MJ, Alatsatianos M, DeAngelis RA, Roche PA, Magotti P, et al. (2010). Complement-mediated inhibition of neovascularization reveals a point of convergence between innate immunity and angiogenesis. *Blood* **116**, 4395–4403.

[64] Pereira R, Halford K, Sokolov BP, Khillan JS, and Prockop DJ (1994). Phenotypic variability and incomplete penetrance of spontaneous fractures in an inbred strain of transgenic mice expressing a mutated collagen gene (COL1A1). *J Clin Invest* **93**, 1765–1769.

[65] Li D, Yu J, Gu F, Pang X, Ma X, Li R, and Liu N (2008). The roles of two novel *FBN1* gene mutations in the genotype-phenotype correlations of Marfan syndrome and ectopia lentis patients with marfanoid habitus. *Genet Test* **12**, 325–330.

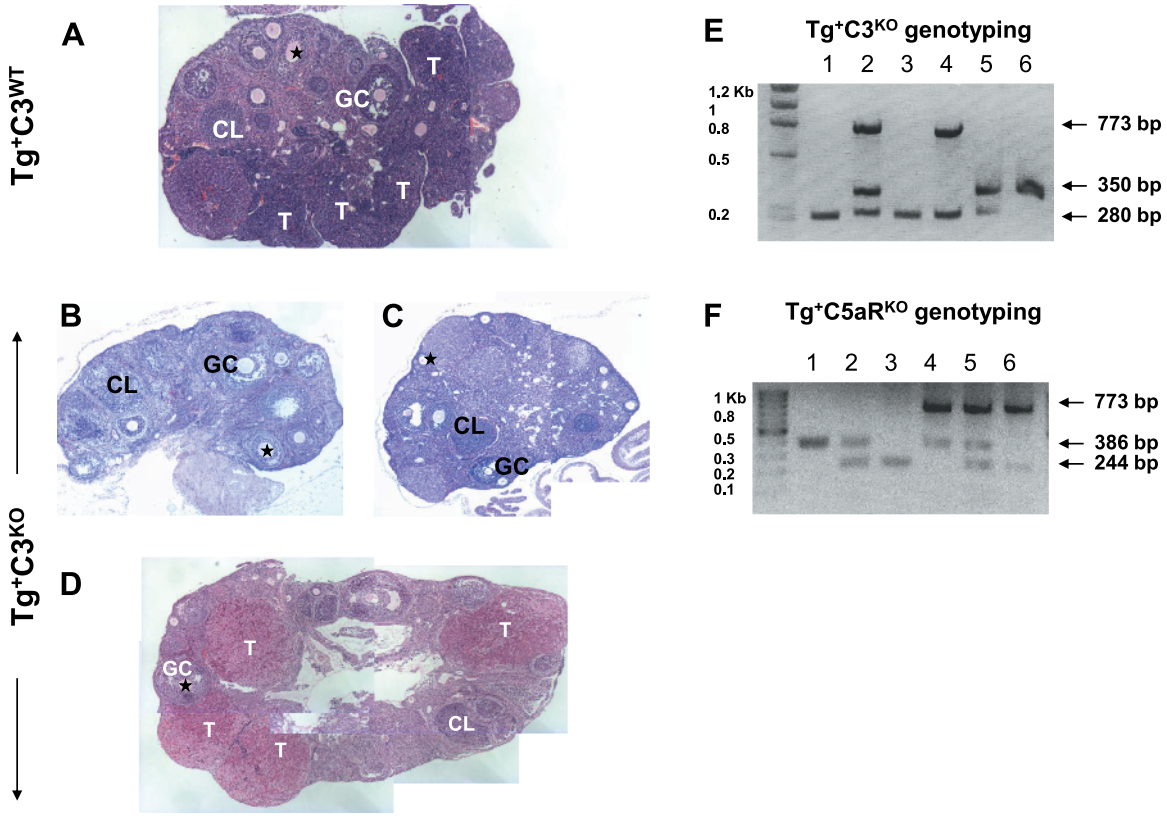

Figure W1. Characterization of mice with genetic complement deficiencies. (A–D) Hematoxylin and eosin–stained frozen sections from ovaries of 16-week-old $Tg^{+}C3^{WT}$ (A) and $Tg^{+}C3^{KO}$ (B–D) mice. Results are representative of 19 $Tg^{+}C3^{WT}$ ovaries and 12 $Tg^{+}C3^{KO}$ ovaries. Stars indicate oocytes. GC, granulosa cells; CL, corpus luteum; T, tumor cells. Original magnification, ×4. (E, F) Genotyping was performed by PCR on genomic DNA using conditions and primers previously described by Connolly and colleagues to detect the insertion of MISIIR (773 bp) and by the Jackson Laboratory to detect intact C3 (350 bp), C3 deficiency (280 bp), intact C5aR (386 bp), and C5aR deficiency (244 bp). (E) 1) $Tg^{-}C3^{KO}$; 2) $Tg^{+}C3^{HET}$; 3) $Tg^{-}C3^{KO}$; 4) $Tg^{+}C_{5a}R^{WT}$; 5) $Tg^{-}C_{5a}R^{HET}$; 6) $Tg^{-}C_{5a}{}^{KO}$. (F) 1) $Tg^{-}C5aR^{WT}$; 2) $Tg^{-}C5aR^{HET}$; 3) $Tg^{-}C5aR^{KO}$; 4) $Tg^{+}C_{5a}R^{WT}$; 5) $Tg^{-}C_{5a}R^{HET}$; 6) $Tg^{-}C_{5a}R^{KO}$.